Chemical disorder and charge transport in ferromagnetic manganites

W. E. Pickett and D. J. Singh

Naval Research Laboratory, Washington, D.C. 20375-5345

(Received 4 February 1997)

Disorder broadening due to randomly distributed La^{3+} and A^{2+} (A=Ca,Sr,Ba) cations is combined with a virtual-crystal treatment of the average system to evaluate the effects on both majority and minority transport in the ferromagnetic $La_{2/3}A_{1/3}MnO_3$ system. The low-density minority carriers which lie in the band tail are localized by disorder, while the majority carriers retain long mean free paths reflected in the observed strongly metallic conductivity. In addition to obtaining transport parameters, we provide evidence that local distortions are due to nearby ionic charges rather than to ion size considerations. [S0163-1829(97)51914-X]

La-based manganites of the type $La_{1-x}A_xMnO_3$ (A=Ca,Sr,Ba) display negative colossal magnetoresistance (CMR) behavior[1,2] for $x \approx \frac{1}{3}$ near the Curie temperature (T_C). This unusual behavior has stimulated avid study of the nonconducting, polaronlike regime above T_C and attempts to model the regime of CMR behavior and the transition to the ferromagnetic metal. So far, however, the low T regime, where these manganites become remarkably good metals, has been largely overlooked. Residual resistivities $\rho_o \sim$ 50–100 $\mu\Omega$ cm have been reported for various manganites,[3–5] and single crystals of (La,Sr)MnO$_3$ for $x=\frac{1}{3}$ have ρ_o=35 $\mu\Omega$ cm.[6] These values are highly metallic for a class of oxides with some members having resistivities eight orders of magnitude larger above T_C. In this paper we address this high-conductivity regime, obtain the disorder broadening arising from cationic disorder, and demonstrate that scattering processes will be highly focused due to the geometry of the majority Fermi surface.

Our approach is, first, to evaluate a realistic electronic structure for an average periodic system with the correct carrier density, and second, to use supercell methods to evaluate the main effects of disorder. Neglecting grain boundary and magnetic domain effects, which can be minimized with the use of single-crystal thin films, the main effects of disorder are the cation charge disorder (viz., La^{3+} vs Ba^{2+}), possible mixed-valence (Mn^{3+}-Mn^{4+}) disorder effects, and local distortions. We find that the cation charge disorder dominates the tendency toward mixed valence. We report also initial indications of the effects of local structural distortions. The small fluctuation of the Mn valence that we obtain is consistent with the high conductivity. Strong metallicity in itself indicates that fluctuations in the Mn charge state are so rapid that an intermediate-valence description such as ours is more appropriate than a mixed-valence description.

To study the manganites we use first-principles local-density functional methods[7–10] with calculational procedures as described elsewhere[11,12] and treat the ferromagnetic cubic perovskite structure (except where noted).[13] This approach describes the end-point compounds properly, as verified by other groups.[14,15] We apply a virtual-crystal (VC) approximation, wherein replacement of $\frac{1}{3}$ of La ions randomly by Ba is modeled by a nucleus equal to the average charge $Z_{VC} = \frac{2}{3}Z_{La}+\frac{1}{3}Z_{Ba}=56\frac{2}{3}$. The valence electronic structure should

also be representative of Sr or Ca substitution of La, since they are isovalent with Ba and are fully ionized. This VC treatment allows the change in carrier density to be treated explicitly and self-consistently.[16] We obtain information about local Mn-site potentials in the disordered system by studying ordered supercells of (La,Ca)MnO$_3$.[11,12] The only previous attempt to identify the effects of disorder from electronic structure studies was by Butler *et al.*,[18] who applied the coherent potential approximation to the La/Ca sublattice in (La,Ca)MnO$_3$. Within the coherent potential approximation, the La^{3+} and Ca^{2+} ions are replaced with a potential with the same average scattering properties. This approach addresses randomness on the cation sublattice self-consistently, but it neglects the distinction between tripositive and dipositive ions that we retain in our supercell studies and find to be crucial.

We first point out the principal features of the VC system. The majority channel has two strongly dispersing e_g-derived $dp\sigma$ bands crossing the Fermi-level (E_F) characteristic of highly metallic behavior. In the minority channel there is a gap between O $2p$ bands and Mn $3d$ bands that extends very near E_F. While E_F falls near the middle of the majority bands of 3 eV band width, the occupied minority band width is only W_{occ}=0.15 eV.

The differences between VC and $x=\frac{1}{3}$ supercell arise because of the two distinct Mn sites in the supercell: Mn_{La-La} is coordinated with eight La^{3+} ions, while Mn_{La-Ca} is coordinated by four La^{3+} ions and four Ca^{2+} ions. Distinct band edges, differing by $\delta\epsilon_d$=0.5 eV, are associated with Mn_{La-La} and with Mn_{La-Ca}. This difference in site energy can be established independently by comparing core-level eigenvalues. This difference in d-site energy can be ascribed directly to a screened Coulomb potential $\Delta\epsilon_d=\Delta Q/\varepsilon R$, where $\Delta Q=4e$ is the difference in charge on the A sites and $R=\sqrt{3}a/2$ is the separation. This gives a local screening factor $\varepsilon \approx 10$, reflecting strong polarizability of the Mn d-O p complex. We use this screening factor to calculate the distribution of site energies in a crystal with random La^{3+} and A^{2+} sites for $x=\frac{1}{3}$. In Fig. 1 we show the distribution of site energies obtained by accounting for both first and second shells of A-site ions. (We use the same screening factor, since their distances differ by only 13%.) The relative prob-
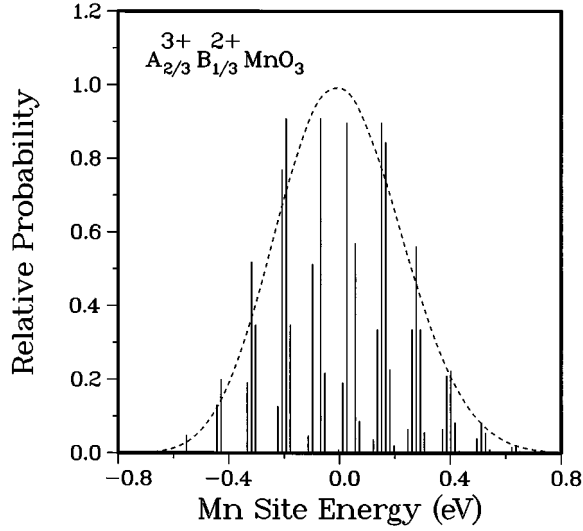
FIG. 1. Distribution of Mn-site screened Coulomb energies (vertical lines) arising from random distribution of La^{3+} ions (with $\frac{2}{3}$ probability) and A^{2+} ions (with $\frac{1}{3}$ probability) on first and second neighbor sites in the perovskite lattice. The dashed line shows the distribution when broadened by 0.1 eV, illustrating its symmetrical variance around the virtual-crystal value (taken as the zero of energy).

ability shown in Fig. 1 is the product of multiplicity of a configuration and the probability of its occurrence subject to the mean concentration $x = \frac{1}{3}$. The full width at half maximum of the distribution is $\delta\epsilon_d = \langle \Delta\epsilon_d \rangle = 0.6$ eV. Because $\delta\epsilon_d \gg W_{occ}$, the low density of minority carriers will lie below the mobility edge[17] and thereby are rendered immobile by strong disorder. This is our first important observation: we have established that these manganites will be half metallic at low T, with conduction limited to a single spin channel, as has been speculated earlier.[11,18]

In addition to quantitative disorder effects, transport properties require the knowledge of Fermi surface (FS) properties. There are two majority channel FS's. A Γ-centered sphere contains 0.05 electron with velocity $v_F^{sph} = 7.1 \times 10^7$ cm/sec, and contributes a Fermi level density of states (DOS) $N^{sph}(E_F) = 0.09$ states/eV-cell. This surface is nearly perfectly spherical with $k_F = 0.45\pi/a$. The other FS is an R-centered cube containing 0.55 holes that touches (due to symmetry) the Γ-centered sphere along the (111) directions. The cube approximates an ideal cube with slightly rounded corners (see below), has an rms velocity $v_F^{cube} = 7.6 \times 10^7$ cm/sec that is nearly constant over the cube faces, and Fermi-level DOS $N^{cube}(E_F) = 0.38$ states/eV-cell. The combined Drude plasma energy $[\hbar^2\Omega_p^2 = (4\pi e^2/3)N(E_F)v_F^2]$ is $\hbar\Omega_p = 1.9$ eV.

These FS properties indicate a moderate density of highly itinerant carriers. Since the majority band width is 3 eV and is much larger than the disorder energy scale $\delta\epsilon_d$, transport in the majority channel should be similar to that of metallic alloys as $T \to 0$. Using $\rho_o = 4\pi/\Omega_p^2\tau_o$, we obtain a defect broadening $\hbar/\tau_o = 18$ meV for a residual resistivity $\rho_o = 35$ $\mu\Omega$ cm.[6] This corresponds to a disorder limited mean-free path $\ell_o = v_F\tau_o \approx 280$ Å, i.e., 75 times the lattice constant, which verifies that this picture is a consistent one. At finite
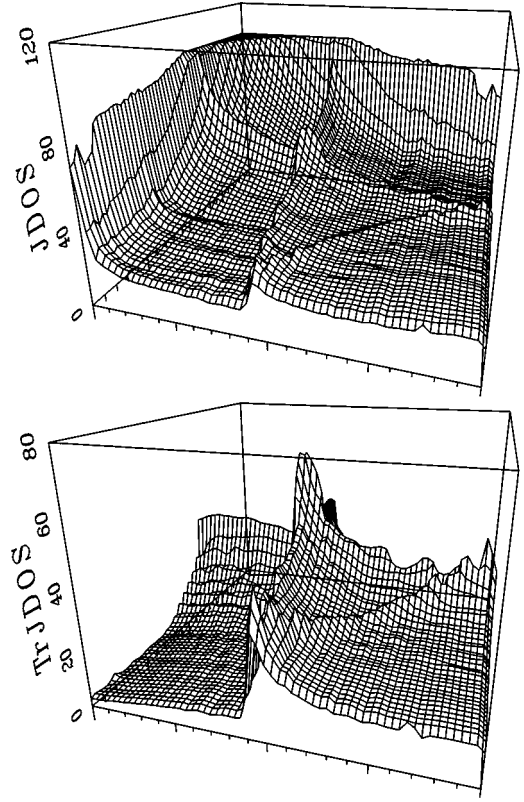

FIG. 2. Unweighted $[\xi(Q),$ top] and transport $[\xi_{tr}(Q),$ bottom] joint density of states (JDOS) for Fermi-surface scattering on the cube majority Fermi surface of the $x = \frac{1}{3}$ virtual crystal, plotted in the Γ-X-M plane. The trivial divergence in $\xi(Q)$ at the Γ point (far left corner) of the JDOS is truncated for plotting. The very narrow ridge along the Cartesian axes in the JDOS reflects the skipping processes, discussed in the text, which are killed by velocity factors in the TrJDOS.

temperature phonons and spin waves become thermally excited. However, since these materials are half metallic, normal emission or absorption of spin waves is forbidden, because the carriers have no conducting minority states at low energy to spin-flip scatter into.[19] Therefore, the low T scattering is due to phonons or to spin-conserving electron-electron processes.

Both of these scattering processes will be affected by the geometry and (an)isotropy of the FS. For the sphere FS the consequences are well known: a weak singularity occurs in the susceptibility at $2k_F$. Consequences are much greater for the large cube FS, because the broad flat faces bring in aspects of one-dimensional processes. In Fig. 2 we show the scattering susceptibility[20]

$$\xi(Q) = \sum_k w_{k,Q}\delta(E_k)\delta(E_{k+Q}) \propto \oint_{\mathcal{L}_Q} \frac{w_{k,Q}dl_k}{|\vec{v}_k \times \vec{v}_{k+Q}|}, \quad (1)$$

where E_k is the band dispersion relation, $\vec{v}_k = \nabla_k E_k$, and $\mathcal{L}_Q$ is the closed curve of intersection of the undisplaced FS and a FS displaced by Q. For weight factor $w = 1$, $\xi(Q)$ gives the amount of phase space for scattering processes beginning and ending on the FS. It has a trivial divergence for

$Q \to 0$. For weight factor $w_{\vec{k},\vec{Q}} = (\vec{v}_k - \vec{v}_{k+Q})^2/2v_F^2$, which reflects how greatly the scattering process degrades the current, the result is the transport analogue $\xi_{tr}(Q)$, and the divergence is canceled by the weight factor.

The flat faces of the cube FS lead to "skipping"-type nesting that was noted earlier for the flat quasi-one-dimensional parts of FS of cuprates.[20,21] There is a large amount of phase space for scattering processes that take a carrier from $\vec{k}$ with velocity $\vec{v}_k$ to $\vec{k}+\vec{Q}$ with velocity $\vec{v}_{k+Q} = \vec{v}_k$ on the same face, with $\vec{Q}$ of the form $(Q_x, Q_y, 0)$ (i.e., displacement parallel to a cube face) with Q not too large. These processes show up most strongly as the very sharp ridge along the cubic axes in Fig. 2. Since $\Sigma_Q \xi(Q) = N(E_F)^2$ reflects the total number of FS scattering processes, the cube FS geometry strongly focuses scattering processes to particular values of $\vec{Q}$. Conventional nesting features are evident in $\xi(Q)$ at $\vec{Q} = (2k_{F,r}, 0, 0)$ in Fig. 2, where $2k_{F,r} = 0.38\pi/a$ is the distance across the cube FS ($2k_F = 2 \times 0.81\pi/a$), reduced (i.e., *umklapped*) to the first Brillouin zone. One only need consider the geometry of the cube to realize scattering is substantial when any Cartesian component of $\vec{Q}$ is equal to $2k_{F,r}$.

For transport processes, the velocity-dependent weight factor has the effect of *killing* the skipping processes, easily seen in Fig. 2, because $\vec{v}_k = \vec{v}_{k+Q}$. Conversely, the conventional nesting processes are enhanced because the velocities are antiparallel. Because $\Sigma_Q \xi_{tr}(Q) = N(E_F)^2$ as well, the weight of the skipping scattering events in $\xi(Q)$ has to reside elsewhere in the zone, and much of it is moved into the conventional nesting ridge in $\xi_{tr}(Q)$. The result is that, for electron-phonon scattering, it is primarily the phonons with any component of $\vec{Q}$ near $2k_{F,r}$ that limit the conductivity. The sphere FS couples with other $Q \lesssim 2k_F$ phonons but the weight is small because of the three-dimensional character and its small contribution to $N(E_F)$.

Structural distortions have been implicated in the behavior of the $x = \frac{1}{3}$ materials by several workers. We have found that the various results reported above, obtained for a cubic crystal structure, still hold when the observed lattice distortion is taken into account. For other band fillings, changes due to structural distortions are more important, and these will be presented elsewhere.

Because electron-phonon coupling is observed to be strong in the manganites,[22] Kohn anomalies will occur at $2k_{F,r}$, and imply a tendency toward charge-density wave formation at $2k_{F,r}$. Structural changes attributed to charge ordering have been observed in the manganites, but so far only at smaller or larger values of x where the system is not highly metallic.[23] Commensurate to incommensurate charge ordering was reported in (La,Ca)MnO$_3$ at $x = \frac{1}{2}$.[24] Due to the lack of single spin-flip processes in a half-metallic material, there will be no Kohn anomalies in the spin wave spectrum.

In a half-metallic ferromagnet near $T = 0$ no spin-flip processes occur, while as T_C is approached spin-flip processes become strong. The NMR spin-lattice relaxation rate will be an excellent experimental monitor of the temperature-dependent variation between these two limits. As the temperature is lowered from T_C toward the half-metallic phase at low temperature, the opening of a "spin gap" should be observable as a decrease in the spin-lattice relaxation rate. We are not aware of reports of such experiments. Very recently, the difference in magnetotransport behavior between single-crystal and polycrystal samples of La$_{1/3}$Sr$_{2/3}$MnO$_3$ has been attributed[6] to spin-polarized tunneling between nearly completely polarized grains. This behavior is what would be expected from a half-metallic ferromagnet.

Now we return to the consideration of local environment variations, both magnetic and structural. The two distinct Mn sites in the supercell also have somewhat different charges and moments. The charge on Mn$_{La-La}$ is only 0.05 electrons larger than on Mn$_{La-Ca}$. Because this charge difference is almost entirely in the majority states, the moment on Mn$_{La-Ca}$ ($3.08\mu_B$) is larger by $0.05\mu_B$. These differences provide the scale for charge and spin fluctuations due to local environment variations; i.e., they are an order of magnitude smaller than suggested by formal valence arguments (which would be more applicable to an insulating phase). Following the arguments above for the distribution of site energies, the variance of the local moment on the Mn ion is $\approx 0.1\mu_B$ for $x = \frac{1}{3}$.

Atomic relaxation of the supercell also gives an indication of the character and magnitude of local distortions in a (La,Ca)MnO$_3$ alloy. In the 3×1 cell (A-site layers of the form ...La-Ca-La-La-Ca-La...) four sites are allowed by symmetry to relax off their ideal perovskite positions: Mn$_{La-Ca}$, La, and the oxygen ions in these two layers, denoted by O$_{La-Ca}$ and O$_{La}$. We have relaxed these degrees of freedom until the energy of the system is minimized. The gain in energy by relaxation is 0.3 eV, of which 0.04 eV can be assigned to an increase in exchange energy due to the increase in moment by $0.13\mu_B$.

The direction of relaxation can be accounted for simply by considering ionic charges in the local environment. Most notable is the buckling of the MnO$_2$ plane between the La and Ca layers, with the Mn-O-Mn bonding angle becoming 176°. This buckling is driven by the displacement of O$_{La-Ca}$, which relaxes by 0.09 Å *toward* the La layer, which has the higher positive charge, rather than towards the Ca layer, which has more available space. The Mn$_{La-Ca}$ ion in the same layer relaxes (by 0.03 Å) toward the Ca layer, which is less repulsive than the La layer. The relaxation of the O$_{La}$ ion is negligible, while the La ion relaxes by 0.08 Å toward the (relaxed, and therefore nearer) Mn$_{La-Ca}$ ion. These observations indicate that local relaxations are determined primarily by local charges, and secondarily by ionic size. Direct Jahn-Teller effects are not observed in these relaxations, possibly because only a few degrees of relaxational freedom were allowed.

In this paper we have presented effects of cation site disorder on the electronic, magnetic, and structural properties of $x = \frac{1}{3}$ manganites. The picture we present accounts for the unexpectedly high conductivity in the ferromagnetic phase, and provides quantitative evidence for the localization of minority carriers lying in the band tail below the mobility edge.

[1] R. von Helmolt *et al.*, Phys. Rev. Lett. **71**, 2331 (1993).

[2] S. Jin *et al.*, Science **264**, 413 (1994).

[3] H. Kuwahara *et al.*, Science **270**, 961 (1995).

[4] A. Urushibara *et al.*, Phys. Rev. B **51**, 14 103 (1995).

[5] J. M. D. Coey *et al.*, Phys. Rev. Lett. **75**, 3910 (1995).

[6] H. Y. Hwang *et al.*, Phys. Rev. Lett. **77**, 2041 (1996).

[7] O. K. Andersen, Phys. Rev. B **12**, 3060 (1975).

[8] S. H. Wei and H. Krakauer, Phys. Rev. Lett. **55**, 1200 (1985).

[9] D. J. Singh, Phys. Rev. B **43**, 6388 (1991).

[10] D. J. Singh, *Planewaves, Pseudopotentials, and the LAPW Method* (Kluwer Academic, Boston, 1994).

[11] W. E. Pickett and D. J. Singh, Phys. Rev. B **53**, 1146 (1996).

[12] W. E. Pickett and D. J. Singh, Europhys. Lett. **32**, 759 (1995).

[13] We have verified that the results discussed in this paper are not altered appreciably if the observed orthorhombic structure is used in the calculations.

[14] N. Hamada, H. Sawada, and K. Terakura, in *Spectroscopy of Mott Insulators and Correlated Metals*, edited by A. Fujimori and Y. Tokura (Springer-Verlag, Berlin, 1995), pp. 95–105.

[15] S. Satpathy, Z. S. Popvić, and F. R. Vukajlović, Phys. Rev. Lett. **76**, 960 (1996).

[16] Treating correlations effects beyond local density approximation has been discussed, and both pro and con arguments have been given: S. Satpathy *et al.*, in Phys. Rev. Lett. **76**, 960 (1996); I. Solovyev *et al.*, Phys. Rev. B **53**, 7158 (1996).

[17] I. Lifshitz, S. A. Gredeskul, and L. A. Pastur, *Introduction to the Theory of Disordered Systems* (Wiley, New York, 1988), Sec. 4.3.

[18] W. H. Butler, X.-G. Zhang, and J. M. MacLaren, in *Magnetic Ultrathin Films, Multilayers, and Surfaces*, MRS Symposium Proceedings No. 384, edited by E. E. Marinero *et al.* (Materials Research Society, Pittsburgh, 1995), pp. 439–443.

[19] V. Yu. Irkhin and M. I. Katsnelson, Usp. Fiz. Nauk **164**, 705 (1994) [Phys. Usp. **37**, 659 (1994)].

[20] W. E. Pickett, H. Krakauer, and R. E. Cohen, Physica B **165&166**, 1057 (1990).

[21] H. Krakauer, W. E. Pickett, and R. E. Cohen, Phys. Rev. B **47**, 1002 (1993).

[22] A. J. Millis, Phys. Rev. B **53**, 8434 (1996); P. Dai *et al.*, *ibid.* **54**, R3694 (1996).

[23] B. J. Sternlieb *et al.*, Phys. Rev. Lett. **76**, 2169 (1996); A. P. Ramirez *et al.*, *ibid.* **76**, 3188 (1996); S. J. L. Billinge *et al.*, *ibid.* **77**, 715 (1996).

[24] C. H. Chen and S.-W. Cheong, Phys. Rev. Lett. **76**, 4042 (1996).